Palestine Journal of Mathematics

Vol. 12(2)(2023) , 578–596

HAAR WAVELET ALGEBRAIC MULTIGRID METHOD FOR THE NUMERICAL SOLUTION OF SQUEEZE FILM LUBRICATION PROBLEM OF POROUS JOURNAL BEARINGS WITH COUPLE STRESS FLUID

S. C. Shiralashetti and Praveenkumar Badiger

Communicated by Suheil Khoury

MSC 2010 Classifications: Primary 65T60, 65Nxx; Secondary 76D08.

Keywords and phrases: Haar wavelet filters, Finite difference, Multigrid, lubrication, journal bearings, Reynolds equation.

The authors would like to thank University Grants Commission (UGC), New Delhi, for supporting this work partially through UGC-SAP DRS-III for 2016-2021: F.510/3/DRS-III/2016 (SAP-I). Also, we thank Karnatak University Dharwad (KUD) for supporting this work under University Research Studentship (URS) 2017-2020: KU/URS/2019/351 Dated: 25/07/2019.

Abstract The proposed article aims to analyze the Haar wavelet algebraic multigrid method for the numerical solution of squeeze film lubrication problem of porous journal bearings with couple stress fluid. To ensure the applicability and efficiency of the proposed method initially elliptic partial differential equations having the exact solutions are presented as the test problems. The acquired findings are displayed through figures and tables to elucidate that, the proposed method is more efficient and promising with the consumption of lesser computational CPU time as compared with the existing methods are Finite difference method, Multigrid method, and Haar wavelet multigrid method. Using the proposed method numerical results of the squeeze film lubrication problem of porous journal bearings with couple stress fluid with the different parameter values are obtained and it is presented in the form of tables and figures.

1 Introduction

During the last few decades, hydrodynamic squeeze film lubrication and its corresponding consequences have been of great interest to research due to its ability to describe various complex phenomena that arise in real life [1]. When the two lubricated surfaces interact along with the normal velocity produces the hydrodynamic squeeze film phenomena with the pressure in the fluid. This phenomenon is also called the positive squeeze effect and the lubricating film is called the squeeze film. During the process of interaction, the viscous lubricant present between these surfaces is not squeezing rapidly but squeezed out in a limited duration. Due to the presence of viscous lubricant property of resistance the pressure is built during this limited period then the load is supported by the lubricant film on the bearing surfaces of the machine components. More precisely, the technology of squeeze films on the bearings has attracted many young researchers due to its widespread applications in many engineering practices, such as jet engines, disc dampers, clutches, machine tools, gears, and human joints. It should be emphasized that there is an enormous of investigations into porous and non-porous squeeze films, Pinkus et al. [2], Cameron [3], Hamrock [4], and many more [5, 6, 7, 8], have been analyzed the squeeze film journal bearings with Newtonian lubricant.

Nowadays, porous journal bearings are broadly used in the industry, since the main advantage of porous bearing is maintenance-free, offers high precision, produces low noise levels, and possesses low friction values, all for relatively low production costs. These bearings are performing satisfactorily for long periods with no external supply of lubricant. The study of hydrodynamic lubrication of porous bearings with the aid of a mathematical model is done by Morgan et al. [9]. Rhodes et al. [10] investigated the modified narrow porous bearings with sealed end pores to prevent the flow of lubricant and this leads to an increase in the load capacity

of the bearing to maintain its self-lubricating features. Also, after the study of narrow porous bearings, Rhodes et al. analyzed the performance of partial porous metal bearings under steady state operating conditions with full film lubricant [11]. Capone [12] has given a solution for a long bearing using the Cameron and Morgan assumption of a linear pressure gradient within the porous bearing material. Porous slider bearing with slip velocity is described by Patel et al. [13]. Also, they found that the permeability parameter and the slip parameter affect the performance of the porous slider bearing. Bhat in his article [14] concludes that the porous inclined slider bearing has a lesser load carrying capacity and less friction than the corresponding porous composite slider bearings by developing the analytical solution for hydrodynamic lubrication of porous composite slider bearing.

Recently, numerical methods play a significant role in finding the solution of the differential equations prescribing diverge phenomena arising in science and engineering. Especially the classical methods like FDM and FEM discretize the differential equations into a system of algebraic equations [15, 16]. The multigrid method is used for the large linear system to minimize the error obtained by the known iterative techniques like Gauss-seidel, Jacobi method, or Relaxation method [17, 18]. Later, Stüben [19] designed the algebraic multigrid method with the aid of principles of the multigrid method for the solution of the large linear system. Brandt in [20] discussed the theory of the algebraic multigrid method for symmetric matrices. Pereira et al. [21] discussed the algebraic multigrid method for different matrices, and conclude that the algebraic multigrid method reduces solving time as compared with the conjugate gradient method. Lepik [22] used the Haar wavelets method for the solution of burgers and Sine-Gordon equations, Shiralashetti et al. [23] used the Chebyshev wavelet method for the study of the effect of couple stress fluid on the squeeze film lubrication in long porous journal bearings. The solution of two dimensional Sobolev and regularized long wave equations in fluids using the Hermite wavelet method has been analyzed by Oruç [24]. The connection between wavelets and the multigrid method by multiresolution analysis is done by Briggs et al. [25]. Wavelet based multigrid method for the solution of the linear and nonlinear elliptic partial differential equation is described in [26]. Leon in [27] described the Haar wavelet multigrid method for the solution of elliptic problems with highly oscillatory coefficients and also concludes that when the standard multigrid method fails to converge in finer mesh size, the wavelet multigrid method does ensure such convergence. The comparative study of wavelet multigrid and FDM in terms of computational time required to obtain the solution of differential equations are studied by Shiralashetti et al. [28, 29, 30]. Garcia et al. [31] studied the wavelet based algebraic multigrid method to find the solution of differential equations. Now, this article presents an application of the Haar wavelet algebraic multigrid method to solve the squeeze film lubrication problem of porous journal bearings with couple stress fluid.

The rest of the work is structured accordingly. The basic definition of Haar wavelets, Haar wavelet multigrid operators and Haar wavelet algebraic multigrid operators are presented in section 2. In section 3, the Haar wavelet algebraic multigrid method of solution is presented for estimating the solutions of elliptic partial differential equations and lubrication problem. Section 4 contains the Haar wavelet algebraic multigrid method of implementation and the mathematical formulation of the lubrication problem. Finally, section 5 contains the conclusion.

2 Mathematical preliminaries of Haar wavelets

Haar wavelets: In 1910 Alfred Haar introduced the Haar wavelet function in the form of regular pulse pair. The Haar wavelet is the simplest and oldest orthonormal wavelet having compact support in [0, 1]. The scaling function and wavelet function of Haar wavelet is defined as

$$\phi(x) = \begin{cases} 1, & if\ 0 \le x < 1, \\ 0, & otherwise. \end{cases} \quad \text{and } \Psi(x) = \begin{cases} 1, & if\ 0 \le x < 1/2, \\ -1, & if\ 1/2 \le x < 1, \\ 0, & otherwise\ . \end{cases}$$

The general relationship between Haar scaling function and Haar wavelets function gives the following Haar wavelets filters coefficients.

$\varphi(x) = \sum_{k=0}^{1} h_k \sqrt{2}\varphi(2x-k)$, and $\Psi(x) = \sum_{k=0}^{1} g_k \sqrt{2}\varphi(2x-k)$.
For Haar Wavelets we have $h_0 = \frac{\sqrt{2}}{2},\ h_1 = \frac{\sqrt{2}}{2},\ g_0 = \frac{\sqrt{2}}{2},\ g_1 = \frac{-\sqrt{2}}{2}$.
Here, h_k are called the low pass scaling filters and g_k are called the high pass wavelet filter coefficients.

Haar wavelet multigrid operators: The general form of the Haar transform matrices that are used as a Haar wavelet multigrid restriction (HR) operator and Haar wavelet multigrid prolongation (HP) operators are given in [32] as,

$$HR = \begin{bmatrix} h_1 & h_0 & 0 & 0 & 0 & 0 & 0 & 0 \\ 0 & 0 & h_1 & h_0 & 0 & 0 & 0 & 0 \\ \vdots & \cdots & \cdots & \cdots & \ddots & \ddots & 0 & 0 \\ 0 & 0 & 0 & 0 & 0 & 0 & h_1 & h_0 \\ g_1 & g_0 & 0 & 0 & 0 & 0 & 0 & 0 \\ 0 & 0 & g_1 & g_0 & 0 & 0 & 0 & 0 \\ \vdots & \cdots & \cdots & \cdots & \ddots & \ddots & 0 & 0 \\ 0 & 0 & 0 & 0 & 0 & 0 & g_1 & g_0 \end{bmatrix}_{\frac{2^J}{2}\times 2^J} \quad and \quad HP = HR^T.$$

Haar wavelet algebraic multigrid operators: In the Haar wavelet multigrid operators both low pass and high pass filters of the Haar wavelet are used to construct the HR, and HP. Similarly the low pass filters, that capture the approximations are used only in the construction of the Haar wavelet algebraic multigrid restriction (HAR) and Haar wavelet algebraic multigrid prolongation (HAP) operators [33]. The general form of these operators is given by

$$HAR = \begin{bmatrix} h_1 & h_0 & 0 & 0 & 0 & \cdots & 0 & 0 \\ 0 & 0 & h_1 & h_0 & 0 & \cdots & 0 & 0 \\ \vdots & & \vdots & & & \cdots & \vdots & \vdots \\ 0 & 0 & 0 & 0 & 0 & \cdots & h_1 & h_0 \end{bmatrix}_{\frac{2^J}{2}\times 2^J} \quad \text{and } HAP = HAR^T.$$

3 Haar wavelet algebraic multigrid method of solution

We now discretize the governing equation of elliptic type with the varied parameters by the finite difference approximations, it reduces differential equation to the difference equation and it can be put in the matrix form as,

$$Ap = b. \tag{3.1}$$

Here, A is the coefficient matrix of order $2^J \times 2^J$ and p, b are column matrices of order $2^J \times 1$. An iterative technique (GMRES [34]) is applied to make the unknown column matrix $[p]_{2^J\times 1}$ to known. Then, the approximate solution $[v]_{2^J\times 1}$ is obtained. Then p can be expressed as $p = v+e$, where e is the error matrix of an order $2^J \times 1$ has to be determined. In connection with this many methods are used to determine and minimize such errors to get an accurate solution. Some of them are multigrid method, Haar wavelet multigrid method and Haar wavelet algebraic multigrid method, etc. We now present the Haar wavelet algebraic multigrid method as follows.
Let, v as the approximate solution of Eq. (3.1), we can write the residual equation as

$$[r]_{2^J\times 1} = [b]_{2^J\times 1} - [A]_{2^J\times 2^J}\,[v]_{2^J\times 1}\,, \tag{3.2}$$

With the aid of Haar wavelet algebraic multigrid operators defined in section 2, we can reduce the required matrices from the finer (J^{th}) level to the coarsest $((J-1)^{th})$ level using the HAR operator. Also, we can construct the matrices back to the finer level from the coarsest level by using the HAP operator. Then from Eq. (3.2), we have,

$$[r]_{2^{J-1}\times 1} = [HAR]_{2^{J-1}\times 2^J}[r]_{2^J\times 1}, \tag{3.3}$$

$$[A]_{2^{J-1}\times 2^{J-1}} = [HAR]_{2^{J-1}\times 2^J}[A]_{2^J\times 2^J}[HAP]_{2^J\times 2^{J-1}}. \tag{3.4}$$

From Eqns. (3.3) and (3.4), we obtain the error equation as

$$[A]_{2^{J-1}\times 2^{J-1}}[e]_{2^{J-1}\times 1} = [r]_{2^{J-1}\times 1}. \tag{3.5}$$

Now, solve the Eq. (3.5) with initial guess $'0'$ gives the error matrix as $[e]_{2^{J-1}\times 1}$.
Again reduce the Eqns. (3.3) and (3.4), we have,

$$[r]_{2^{J-2}\times 1} = [HAR]_{2^{J-2}\times 2^{J-1}}[r]_{2^{J-1}\times 1}, \tag{3.6}$$

$$[A]_{2^{J-1}\times 2^{J-1}} = [HAR]_{2^{J-1}\times 2^{J}}[A]_{2^{J}\times 2^{J}}[HAP]_{2^{J}\times 2^{J-1}}. \tag{3.7}$$

From Eqns. (3.6) and (3.7), the error equation takes the form as

$$[A]_{2^{J-2}\times 2^{J-2}}[e]_{2^{J-2}\times 1} = [r]_{2^{J-2}\times 1}. \tag{3.8}$$

Now, on solving the Eq. (3.8) with initial guess $'0'$ we obtained the error matrix as$[e]_{2^{J-2}\times 1}$.
Continuing the same procedure up to the coarsest level we have

$$[r]_{2\times 1} = [HAR]_{2\times 4}[r]_{4\times 1}, \tag{3.9}$$

$$[A]_{2\times 2} = [HAR]_{2\times 4}[A]_{4\times 4}[HAP]_{4\times 2}. \tag{3.10}$$

From Eqns. (3.9) and (3.10), we have the error equation as,

$$[A]_{2\times 2}[e]_{2\times 1} = [r]_{2\times 1}. \tag{3.11}$$

Now, solve the Eq. (3.11) exactly, we obtain $[e]_{2\times 1}$.
From $[e]_{2\times 1}$, update the solution

$$p_{4\times 1} = [e]_{4\times 1} + [HAP]_{4\times 2}\,[e]_{2\times 1}\,. \tag{3.12}$$

Solve $[A]_{4\times 4}[p]_{4\times 1} = [r]_{4\times 1}$with the initial guess $p_{4\times 1}$.
From $p_{4\times 1}$, update the solution $p_{8\times 1}$ as

$$p_{8\times 1} = [e]_{8\times 1} + [HAP]_{8\times 4}[p]_{4\times 1}. \tag{3.13}$$

Solve $[A]_{8\times 8}\,[p]_{8\times 1} = [r]_{8\times 1}$with the initial guess $p_{8\times 1}$.
Continuing the procedure up to the finer level we have

$$p_{2^{J}\times 1} = [v]_{2^{J}\times 1} + [HAP]_{2^{J}\times 2^{J-1}}[p]_{2^{J-1}\times 1}. \tag{3.14}$$

Finally, Solve $[A]_{2^{J}\times 2^{J}}\,[p]_{2^{J}\times 1} = [b]_{2^{J}\times 1}$ with an initial guess $p_{2^{J}\times 1}$.
Now, the obtained solution $p_{2^{J}\times 1}$ is the required Haar wavelet algebraic multigrid method (HWA MGM) solution of the Eq. (3.1) as the HWAMGM solution of the governing partial differential equation.

4 Haar wavelet algebraic multigrid method of implementation

In this section, initially, we applied the HWAMGM for the numerical solution of the elliptic partial differential equations to check the efficiency of the proposed method, and then we obtained the HWAMGM solution of the squeeze film lubrication problem of porous journal bearings with couple stress fluid flow problem. For the error analysis, we used the formula as, $E_{\max .} = \max |p_e - p_a|$, where p_e is the exact solution and p_a is the approximate solution.

Test Problem 1. Firstly, we consider the two dimensional elliptic partial differential equation with the forcing function as a product of exponential and algebraic function [35] as,

$$\frac{\partial^2 p}{\partial x^2} + \frac{\partial^2 p}{\partial y^2} = e^{-x}\left(x - 2 + y^3 + 6y\right),\ 0 \le x \le 1,\ 0 \le y \le 1. \tag{4.1}$$

Subjected to the boundary conditions,

$$p(x,0) = xe^{-x},\ p(x,1) = e^{-x}(x+1),\ p(0,y) = y^3, p(1,y) = \left(1+y^3\right)e^{-1}.$$

The exact solution of test problem 1 is $p(x,y) = e^{-x}\left(x+y^3\right)$.
Applying the finite difference approximations of the partial derivatives, Eq. (4.1) reduces to the following form,

$$\frac{p_{i-1,j} - 2p_{i,j} + p_{i+1,j}}{\Delta x^2} + \frac{p_{i,j-1} - 2p_{i,j} + p_{i,j+1}}{\Delta y^2} = e^{-x_i}\left(x_i - 2 + y_j^3 + 6y_j\right). \tag{4.2}$$

Where, $i, j = 1, 2, 3, ..., J$, $\Delta x = x_{i+1} - x_i$,and $\Delta y = y_{j+1} - y_j$. For instance, $J = 4$ Eq. (4.2) gives as,

$$[A]_{16\times16}\,[p]_{16\times1} = [\mathrm{b}]_{16\times1}. \tag{4.3}$$

By using GMRES method, we obtained the approximate solution of the Eq. (4.3) as,
$v_{16\times1} = \Big[\ 0 \quad 0.2320 \quad 0.3325 \quad 0.3573 \quad 0.0360 \quad 0.1868 \quad 0.3409 \quad 0.3706$
$0.2878 \quad 0.3721 \quad 0.4725 \quad 0.4632 \quad 0.9713 \quad 0.9280 \quad 0.8311 \quad 0.7147\ \Big]^T$. By Eq. (3.2) we obtained the $[r]_{16\times1}$ as,

$$[r]_{16\times1} = \Big[\ 0 \quad 0.0069 \quad 0.0098 \quad 0.0106 \quad 0.0011 \quad -0.2044 \quad 0.0414 \quad 0.0109$$
$$0.0085 \quad -0.1772 \quad 0.0516 \quad 0.0137 \quad 0.0287 \quad 0.0274 \quad 0.0245 \quad 0.0211\ \Big]^T.$$

From Eq. (3.3) we have $[r]_{8\times1} = [HAR]_{8\times16}\,[r]_{16\times1}$.
The coefficient matrix from Eq. (3.4) becomes $[A]_{8\times8} = [HAR]_{8\times16}\,[A]_{16\times16}\,[HAP]_{16\times8}$.
Again, From Eq. (3.5) the error equation becomes $[A]_{8\times8}[e]_{8\times1} = [r]_{8\times1}$ and solving this error equation with the help of GMRES method with the initial guess $'0'$ we obtain

$$[e]_{8\times1} = \quad [0.0011 \quad 0.0031 \quad 0.1196 \quad -0.0620 \quad 0.1011 \quad -0.0611 \quad 0.0086 \quad 0.0070\ ]^T.$$

From Eq. (3.6) we have $[r]_{4\times1} = [HAR]_{4\times8}.[r]_{8\times1}$.
Also, from Eq. (3.7) we obtain $[A]_{4\times4} = [HAR]_{4\times8}[A]_{8\times8}[HAP]_{8\times4}$.
From Eq. (3.8), the error equation becomes $[A]_{4\times4}[e]_{4\times1} = [r]_{4\times1}$. Again solving this error equation for $[e]_{4\times1}$ with initial guess $'0'$ we have

$$[e]_{4\times1} = \Big[\ 0.0030 \quad 0.0645 \quad 0.0447 \quad 0.0112\ \Big]^T.$$

Continuing the same procedure up to the coarsest level and from Eq. (3.9) we have

$$[r]_{2\times1} = \Big[\ -0.0438 \quad -0.0006\ \Big]^T.$$

From Eq. (3.10), we obtained $[A]_{2\times2} = \begin{bmatrix} 0.5000 & 0.2500 \\ 0.2500 & 0.5000 \end{bmatrix}$.
By Eq. (3.11), we obtained the error equation as,

$$\begin{bmatrix} 0.5000 & 0.2500 \\ 0.2500 & 0.5000 \end{bmatrix} [e]_{2\times1} = \begin{bmatrix} -0.0438 \\ -0.0006 \end{bmatrix}. \tag{4.4}$$

Solving Eq. (4.5) we obtained, $[e]_{2\times1} = \Big[\ -0.1160 \quad 0.0569\ \Big]^T$.
By Eq. (3.12), we obtained, $p_{4\times1} = \Big[\ -0.0790 \quad -0.0175 \quad 0.0849 \quad 0.0514\ \Big]^T$.
Now, solving $[A]_{4\times4}\,[p]_{4\times1} = [r]_{4\times1}$by using GMRES method with
$p_{4\times1} = \Big[\ -0.0790 \quad -0.0175 \quad 0.0849 \quad 0.0514\ \Big]^T$ as an initial approximation and then, we obtained the solution
$[p]_{4\times1} = \Big[\ -0.0217 \quad 0.0527 \quad 0.0652 \quad 0.0511\ \Big]^T$. By Eq. (3.13), we obtained

$p_{8\times1} = \begin{bmatrix} -0.0143 & -0.0122 & 0.1569 & -0.0248 & 0.1472 & -0.0150 & 0.0448 & 0.0431 \end{bmatrix}^T$.
Next, solving the equation $[A]_{8\times8}\,[p]_{8\times1} = [r]_{8\times1}$ by using GMRES method with
$p_{8\times1} = \begin{bmatrix} -0.0143 & -0.0122 & 0.1569 & -0.0248 & 0.1472 & -0.0150 & 0.0448 & 0.0431 \end{bmatrix}^T$ as an initial guess, we obtained the solution
$p_{8\times1} = \begin{bmatrix} -0.0070 & -0.0021 & 0.1509 & -0.0235 & 0.1465 & -0.0232 & 0.0428 & 0.0390 \end{bmatrix}^T$.
Continuing the same procedure up to the finer level and by Eq. (3.14) we obtained

$$[p]_{16\times1} = \begin{bmatrix} -0.0049 & 0.2270 & 0.3310 & 0.3559 & 0.1426 & 0.2934 & 0.3242 & 0.3539 \\ 0.3914 & 0.4757 & 0.4561 & 0.4468 & 1.0016 & 0.9582 & 0.8587 & 0.7422 \end{bmatrix}^T.$$

Finally, solving $[A]_{16\times16}[p]_{16\times1} = [b]_{16\times1}$ with an initial guess $p_{16\times1}$ and then we obtained the solution $p_{16\times1}$, and this HWAMGM solution of the test problem 1 is presented in Table 1 and Figure 1. The maximum error and consumption of computational CPU time for obtaining the solutions are presented in Table 2.

Table 1. Comparison of the numerical solution (FDM, MGM, HWMGM, and HWAMGM) with the exact solution of the test problem 1 for $J = 4$.

x	y	FDM	MGM	HWMGM	HWAMGM	Exact
0	0	0	-7.5265e-03	6.2886e-03	-4.9351e-04	0
0	3.3333e-01	3.5974e-02	-2.5897e-02	1.0337e-01	4.7581e-02	3.7037e-02
0	6.6667e-01	2.8780e-01	6.9433e-02	2.8750e-01	3.0579e-01	2.9630e-01
0	1.0000e+00	9.7131e-01	1.0287e+00	9.7030e-01	1.0002e+00	1.0000e+00
3.3333e-01	0	2.3199e-01	2.1701e-01	2.3636e-01	2.3767e-01	2.3884e-01
3.3333e-01	3.3333e-01	1.8676e-01	1.1250e-01	2.6131e-01	2.4324e-01	2.6538e-01
3.3333e-01	6.6667e-01	3.7212e-01	2.9867e-01	4.2264e-01	4.3129e-01	4.5115e-01
3.3333e-01	1.0000e+00	9.2797e-01	9.6875e-01	9.2700e-01	9.5566e-01	9.5538e-01
6.6667e-01	0	3.3246e-01	2.9632e-01	3.3016e-01	3.4115e-01	3.4228e-01
6.6667e-01	3.3333e-01	3.4088e-01	1.9747e-01	3.8148e-01	3.4048e-01	3.6129e-01
6.6667e-01	6.6667e-01	4.7249e-01	4.0474e-01	4.6738e-01	4.7208e-01	4.9440e-01
6.6667e-01	1.0000e+00	8.3115e-01	8.6337e-01	8.3028e-01	8.5600e-01	8.5570e-01
1.0000e+00	0	3.5733e-01	3.0000e-01	3.5846e-01	3.6668e-01	3.6788e-01
1.0000e+00	3.3333e-01	3.7056e-01	6.6320e-02	4.8940e-01	3.7875e-01	3.8150e-01
1.0000e+00	6.6667e-01	4.6320e-01	5.3705e-01	4.6272e-01	4.7387e-01	4.7688e-01
1.0000e+00	1.0000e+00	7.1465e-01	7.3830e-01	7.1391e-01	7.3641e-01	7.3576e-01

From Table 1 we can observe that the HWAMGM solution for $J = 4$ of test problem 1 is in good agreement with the exact solution as compared with the FDM, MGM, and HWMGM.

Table 2. Comparison of the numerical methods (FDM, MGM, HWMGM, and HWAMGM) maximum error and CPU time (in seconds) of the test problem 1.

Size of the Matrices	Numerical Method	$E_{\max}$.	Time		
			Setup	**Running**	**Total**
16×16	FDM	7.9030e-02	1.9747e+00	6.9917e-02	2.0446e+00
	MGM	3.1518e-01	1.3409e-01	4.4961e-03	1.3858e-01
	HWMGM	1.0789e-01	4.9860e-02	4.7822e-03	5.4642e-02
	HWAMGM	2.2324e-02	3.7773e-02	3.1750e-03	4.0948e-02
64×64	FDM	5.2678e-03	2.9905e+00	8.2981e-02	3.0735e+00
	MGM	4.5176e-04	1.6423e-01	5.8379e-03	1.7007e-01
	HWMGM	4.6017e-03	8.5981e-02	6.9839e-03	9.2965e-02
	HWAMGM	1.7997e-04	8.1502e-02	5.2843e-03	8.6786e-02
256×256	FDM	3.7861e-04	4.1663e+00	8.7348e-02	4.2537e+00
	MGM	6.3103e-05	1.7013e-01	7.1577e-03	1.7728e-01
	HWMGM	5.4995e-05	1.0293e-01	6.4303e-03	1.0936e-01
	HWAMGM	6.3326e-05	9.6951e-02	7.1034e-03	1.0405e-01
1024×1024	FDM	2.7146e-04	5.1242e+00	1.4382e-01	5.2680e+00
	MGM	3.4439e-06	4.9663e-01	6.4619e-02	5.6124e-01
	HWMGM	3.8068e-05	3.5845e-01	7.0009e-02	4.2846e-01
	HWAMGM	3.6545e-08	3.4478e-01	6.6274e-02	4.1105e-01
4096×4096	FDM	2.6293e-05	9.7404e+00	1.5076e+00	1.1248e+01
	MGM	4.5205e-08	1.0783e+01	1.3231e+00	1.2106e+01
	HWMGM	1.3827e-06	9.2164e+00	1.3215e+00	1.2148e+01
	HWAMGM	3.3942e-10	1.0833e+01	1.3152e+00	1.0538e+01

From Table 2 we can see that the maximum error and the computational CPU time of the HWAMGM are lesser as compared with the FDM, MGM, and HWMGM.
Figure 1 represents the solution obtained by FDM, MGM, HWMGM, and HWAMGM solutions for $J = 12$ with the exact solution of the test problem 1.

Test Problem 2. Secondly, we consider the elliptic partial differential equation with the forcing function as the product of exponential, algebraic, and trigonometric function [35] as,

$$\begin{aligned}\frac{\partial^2 p}{\partial x^2} + \frac{\partial^2 p}{\partial y^2} &= e^{\frac{-\alpha x+y}{5}}\left\{\left(\frac{-4}{5}\alpha^3 x - \frac{2}{5} + 2\alpha^2\right)\cos\left(\alpha^2 x^2 + y\right)\right\} \\ &+ e^{\frac{-\alpha x+y}{5}}\left\{\left(\frac{1}{25} - 1 - 4\alpha^4 x^2 + \frac{\alpha^2}{25}\right)\sin\left(\alpha^2 x^2 + y\right)\right\}. \qquad (4.5)\end{aligned}$$

Subjected to the boundary conditions, $p(x,0) = e^{\frac{-\alpha x}{5}}\sin(\alpha^2 x^2)$, $p(x,1) = e^{\frac{1-\alpha x}{5}}\sin(1+\alpha^2 x^2)$, $p(0,y) = e^{\frac{y}{5}}\sin(y)$, $p(1,y) = e^{\frac{y-\alpha}{5}}\sin(\alpha^2+y)$.
Here, $\alpha = 3$, $x, y \in [0,1]$ and the exact solution of test problem 2 is $p(x,y) = e^{\frac{-\alpha x+y}{5}}\sin(\alpha^2 x^2 + y)$.
Applying the finite difference approximations of the partial derivatives, Eq. (4.5) reduces to the linear system and by using the HWAMGM presented in section 3, the obtained numerical solution of test problem 2 and is presented in Table 3 and Figure 2. The maximum error and consumption of computational CPU time for obtaining the solutions are presented in Table 4.
From Table 3 we can observe that the HWAMGM solution for $J = 4$ of test problem 2 is in good agreement with the exact solution as compared with the FDM, MGM, and HWMGM.
From Table 4 we can observe that the maximum error and the computational CPU time of the HWAMGM of the test problem 2 are lesser as compared with the FDM, MGM, and HWMGM.

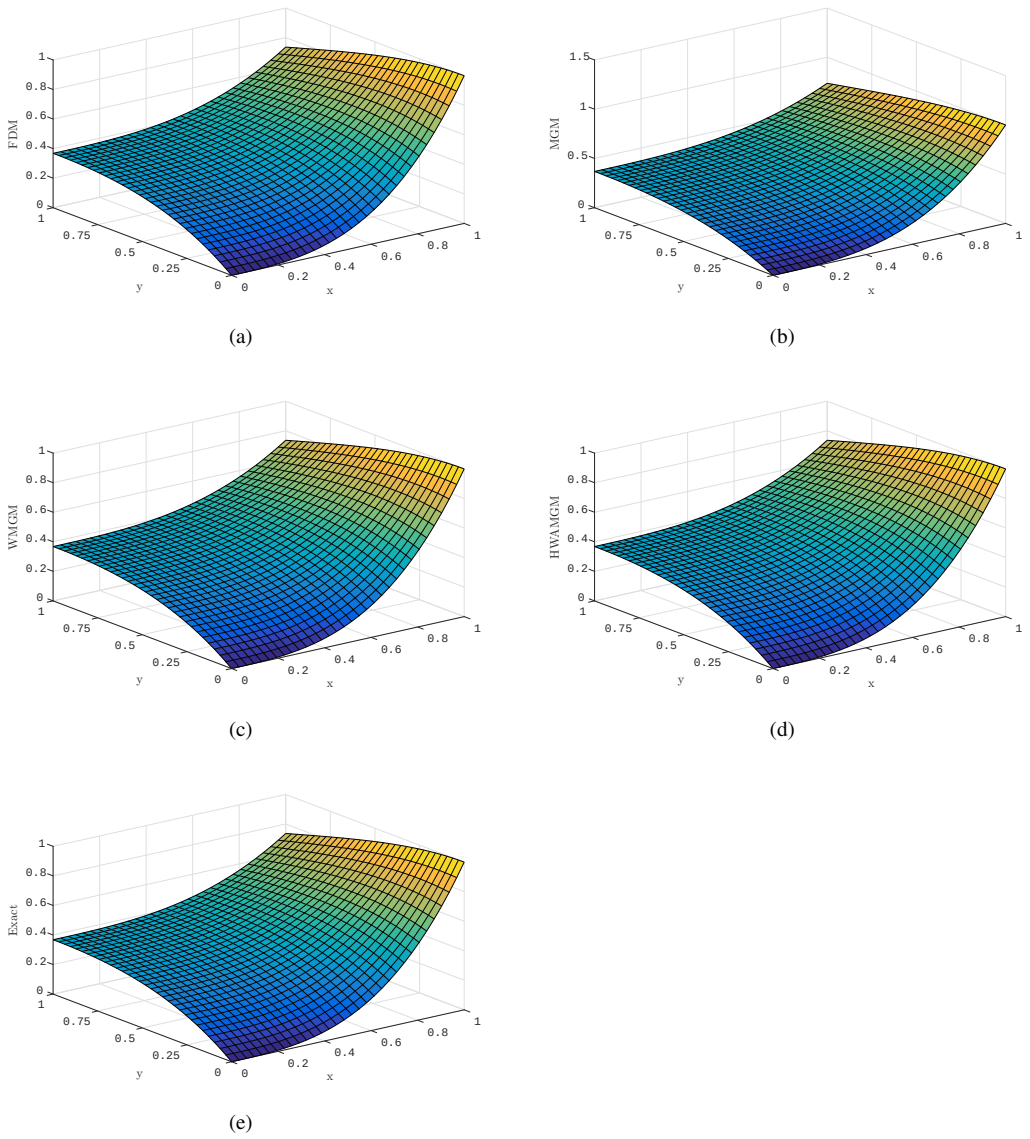

(a) (b) (c) (d) (e)

Figure 1. Numerical methods solution ((a) FDM, (b) MGM, (c) HWMGM, and (d) HWAMGM) with the (e) exact solution of the test problem 1.

Figure 2 represents the solution obtained by FDM, MGM, HWMGM, and HWAMGM solutions for $J = 12$ with the exact solution of the test problem 2.

Test Problem 3. Thirdly, we consider an elliptic partial differential equation with the forcing function as the product of algebraic and exponential function [36] as,

$$\frac{\partial^2 p}{\partial x^2} + \frac{\partial^2 p}{\partial y^2} = \left(x^2 + y^2\right) e^{xy}, \;\; 0 \leq x \leq 2, \;\; 0 \leq y \leq 1. \tag{4.6}$$

Subjected to the boundary conditions,

$$p\left(x, 0\right) = 1, \;\; p\left(x, 1\right) = e^x, \;\; p\left(0, y\right) = 1, \;\; p\left(2, y\right) = e^{2y}.$$

This test problem 3 has the exact solution as $p\left(x, y\right) = e^{xy}$.
Applying the finite difference approximations of the partial derivatives, Eq. (4.6) reduces to the linear system, and by using the HWAMGM presented in section 3, the obtained numerical solution of test problem 3 is presented in Table 5 and Figure 3. The maximum error and consumption of computational CPU time for obtaining the solutions are presented in Table 6.

Table 3. Comparison of the numerical solution (FDM, MGM, HWMGM, and HWAMGM) with the exact solution of the test problem 2 for $J = 4$.

x	y	FDM	MGM	HWMGM	HWAMGM	Exact
0	0	-6.2172e-15	4.8628e-06	-1.4474e-16	-5.9048e-07	0
0	3.3333e-01	3.5048e-01	3.4988e-01	3.4975e-01	3.4998e-01	3.4975e-01
0	6.6667e-01	7.0805e-01	7.0669e-01	7.0789e-01	7.0651e-01	7.0657e-01
0	1.0000e+00	1.0299e+00	1.0278e+00	1.0297e+00	1.0278e+00	1.0278e+00
3.3333e-01	0	6.9038e-01	6.8895e-01	6.8894e-01	6.8894e-01	6.8894e-01
3.3333e-01	3.3333e-01	6.9096e-01	1.9883e-01	2.9428e-01	2.3553e-01	8.5061e-01
3.3333e-01	6.6667e-01	6.2555e-01	3.5919e-01	4.2048e-01	4.0440e-01	9.3121e-01
3.3333e-01	1.0000e+00	9.1121e-01	9.0930e-01	9.1100e-01	9.0930e-01	9.0930e-01
6.6667e-01	0	-5.0836e-01	-5.0732e-01	-5.0730e-01	-5.0730e-01	-5.0730e-01
6.6667e-01	3.3333e-01	-3.6221e+00	-3.8171e+00	-3.7028e+00	-3.6748e+00	-6.6567e-01
6.6667e-01	6.6667e-01	-3.7918e+00	-4.2126e+00	-4.1132e+00	-4.0687e+00	-7.6513e-01
6.6667e-01	1.0000e+00	-7.8675e-01	-7.8510e-01	-7.8657e-01	-7.8510e-01	-7.8510e-01
1.0000e+00	0	2.2665e-01	2.2612e-01	2.2618e-01	2.2618e-01	2.2618e-01
1.0000e+00	3.3333e-01	5.3683e-02	5.3523e-02	5.3571e-02	5.3459e-02	5.3571e-02
1.0000e+00	6.6667e-01	-1.5053e-01	-1.5023e-01	-1.5049e-01	-1.5004e-01	-1.5021e-01
1.0000e+00	1.0000e+00	-3.6543e-01	-3.6467e-01	-3.6535e-01	-3.6467e-01	-3.6467e-01

Table 4. Comparison of the numerical methods (FDM, MGM, HWMGM, and HWAMGM) maximum error and CPU time (in seconds) of the test problem 2.

Size of the Matrices	Numerical Method	$E_{\max .}$	Time		
			Setup	Running	Total
16×16	FDM	7.6504e-04	3.3233e+00	7.7058e-02	3.4004e+00
	MGM	2.0130e-06	8.8822e-02	5.9157e-03	9.4737e-02
	HWMGM	6.8175e-04	3.3820e-02	4.2441e-03	3.8064e-02
	HWAMGM	3.6032e-07	2.7628e-02	3.5661e-03	3.1194e-02
64×64	FDM	5.2190e-07	5.0068e+00	8.1469e-02	5.0883e+00
	MGM	2.8289e-10	1.0754e-01	4.2586e-03	1.1180e-01
	HWMGM	1.3696e-10	6.1979e-02	5.9258e-03	6.7904e-02
	HWAMGM	1.1565e-11	4.9046e-02	4.5164e-03	5.3563e-02
256×256	FDM	4.3287e-08	6.9716e+00	8.6839e-02	7.0585e+00
	MGM	6.9154e-11	2.1328e-01	6.3253e-03	2.1960e-01
	HWMGM	2.2587e-08	8.2609e-02	5.8253e-03	8.8434e-02
	HWAMGM	1.3922e-12	7.9283e-02	5.7001e-03	8.4983e-02
1024×1024	FDM	3.0230e-10	6.7362e+00	2.8817e-01	7.0243e+00
	MGM	1.0122e-11	4.6164e-01	2.5292e-02	4.8693e-01
	HWMGM	2.6911e-09	3.1109e-01	2.8013e-02	3.3911e-01
	HWAMGM	1.5543e-15	2.1119e-01	2.7372e-02	2.3856e-01
4096×4096	FDM	2.3286e-10	1.2260e+01	3.9538e-01	1.2655e+01
	MGM	4.2827e-13	1.3155e+01	2.1823e-01	1.3373e+01
	HWMGM	3.3605e-10	1.3834e+01	2.5425e-01	1.4088e+01
	HWAMGM	5.5511e-17	1.3063e+01	2.1132e-01	1.3274e+01

From Table 5 we can observe that the HWAMGM solution for $J = 4$ of test problem 3 is in good agreement with the exact solution as compared with the FDM, MGM, and HWMGM. From Table 6 we can observe that the maximum error and the computational CPU time of the HWAMGM of test problem 3 are lesser as compared with the FDM, MGM, and HWMGM. Figure 3 represents the solution obtained by FDM, MGM, HWMGM, and HWAMGM solutions for $J = 12$ with the exact solution of the test problem 3.

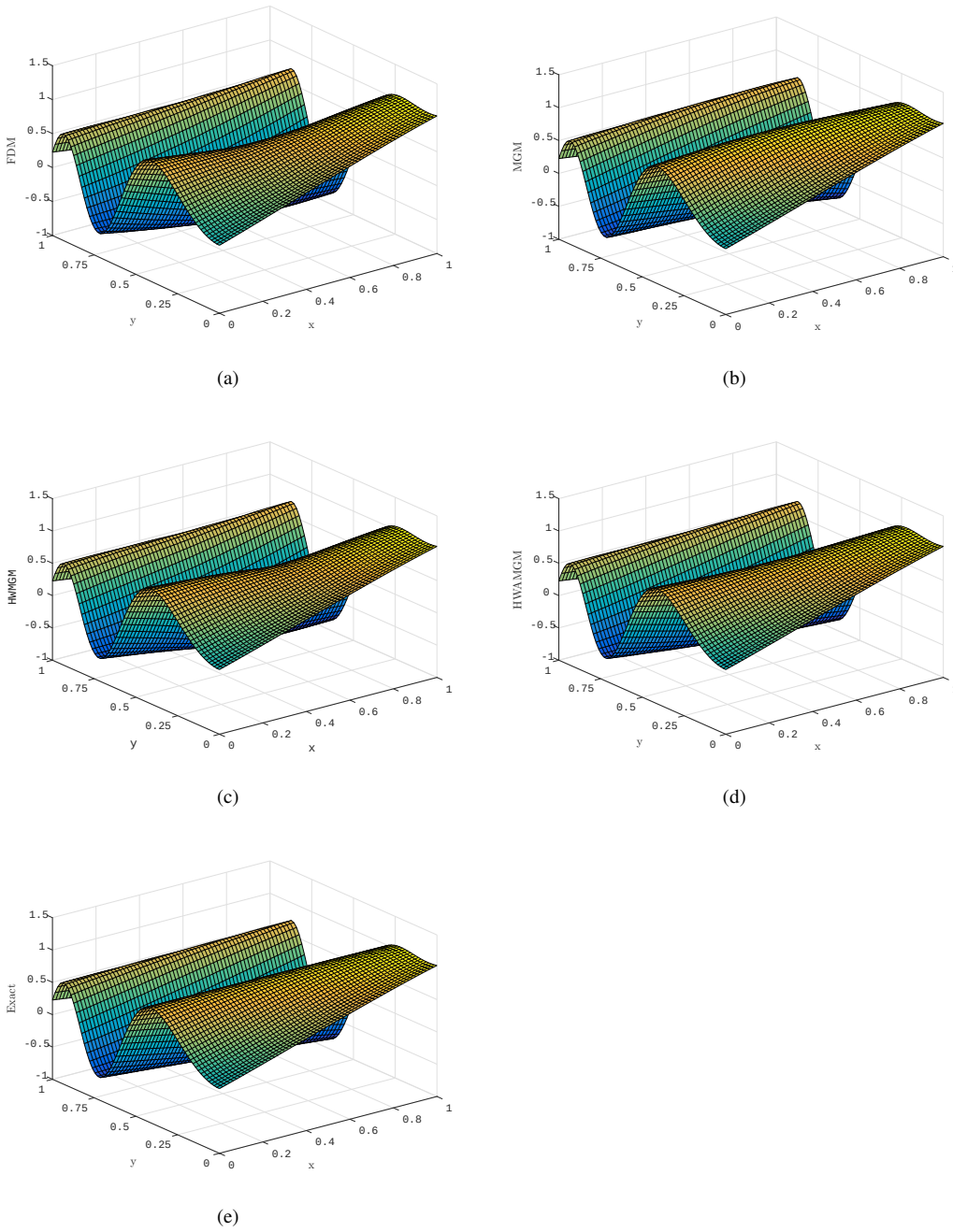

Figure 2. Numerical methods solution ((a) FDM, (b) MGM, (c) HWMGM, and (d) HWAMGM) with the (e) exact solution of the test problem 2.

Lubrication Problem 4. Lastly, we consider the squeeze film lubrication problem of porous journal bearings with couple stress fluid flow Eq. (4.21).

Mathematical Formulation of the Lubrication Problem

Physical configuration of the Lubrication Problem: Figure 4 represents the geometry of the squeeze film bearing with incompressible couple stress fluid as the lubricant in the film region. $\frac{dh}{dt}$ be the velocity of the non rotating journal of the radius R is approaching the bearing surface of thickness H_0. In consideration with the assumptions of the thin-film theory of hydrodynamic lubrication [2] and neglecting the body force and body couples, the momentum equations and the continuity equation for couple stress fluid derived by Stokes [37]. The mathematical formulation

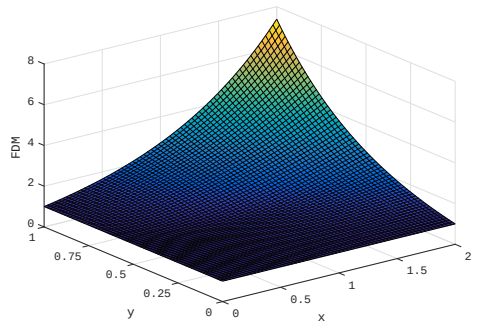

(a)

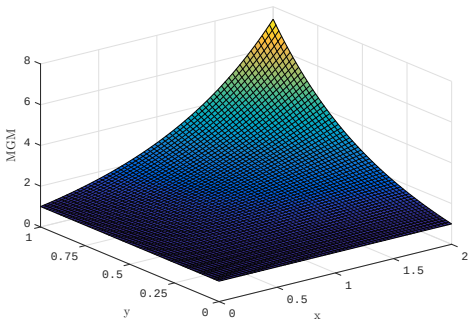

(b)

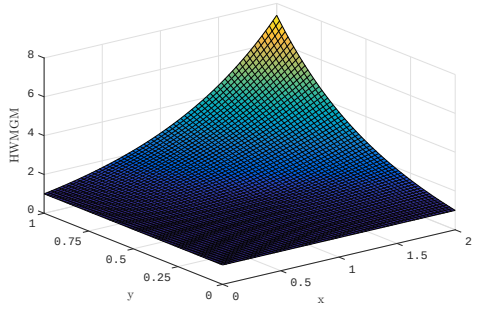

(c)

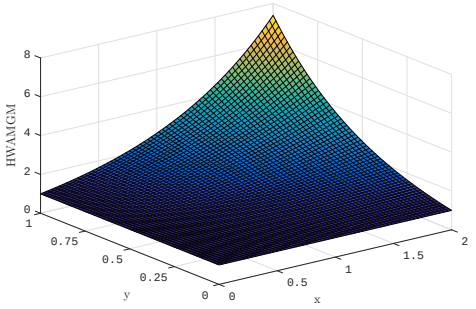

(d)

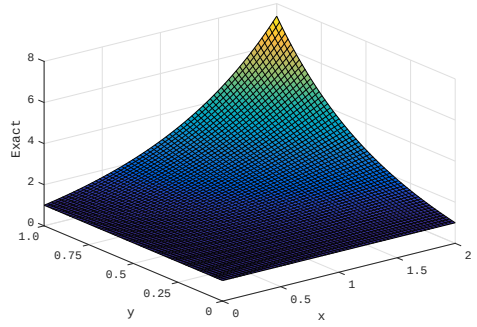

(e)

Figure 3. Numerical methods solution ((a) FDM, (b) MGM, (c) HWMGM, and (d) HWAMGM) with the (e) exact solution of the test problem 3.

Table 5. Comparison of the numerical solution (FDM, MGM, HWMGM, and HWAMGM) with the exact solution of the test problem 3 for $J = 4$.

x	y	FDM	MG	HWMGM	HWAMM	Exact
0	0	9.9991e-01	9.9969e-01	1.0000e+00	1.0000e+00	1.0000e+00
0	3.3333e-01	9.9991e-01	9.9903e-01	1.0000e+00	1.0003e+00	1.0000e+00
0	6.6667e-01	9.9991e-01	9.9838e-01	9.9997e-01	9.9882e-01	1.0000e+00
0	1.0000e+00	9.9991e-01	9.9772e-01	9.9997e-01	1.0000e+00	1.0000e+00
6.6667e-01	0	9.9991e-01	9.9953e-01	1.0000e+00	1.0000e+00	1.0000e+00
6.6667e-01	3.3333e-01	1.1460e+00	1.2436e+00	1.2490e+00	1.2243e+00	1.2488e+00
6.6667e-01	6.6667e-01	1.5404e+00	1.5506e+00	1.5608e+00	1.5377e+00	1.5596e+00
6.6667e-01	1.0000e+00	1.9475e+00	1.9452e+00	1.9477e+00	1.9477e+00	1.9477e+00
1.3333e+00	0	9.9991e-01	9.9936e-01	1.0000e+00	1.0000e+00	1.0000e+00
1.3333e+00	3.3333e-01	1.5845e+00	1.5627e+00	1.5630e+00	1.5436e+00	1.5596e+00
1.3333e+00	6.6667e-01	2.4508e+00	2.4284e+00	2.4378e+00	2.4484e+00	2.4324e+00
1.3333e+00	1.0000e+00	3.7933e+00	3.7907e+00	3.7935e+00	3.7937e+00	3.7937e+00
2.0000e+00	0	9.9991e-01	9.9920e-01	1.0000e+00	1.0000e+00	1.0000e+00
2.0000e+00	3.3333e-01	1.9475e+00	1.9461e+00	1.9477e+00	1.9481e+00	1.9477e+00
2.0000e+00	6.6667e-01	3.7933e+00	3.7911e+00	3.7935e+00	3.7938e+00	3.7937e+00
2.0000e+00	1.0000e+00	7.3884e+00	7.3854e+00	7.3888e+00	7.3891e+00	7.3891e+00

Table 6. Comparison of the numerical methods (FDM, MGM, HWMGM, and HWAMGM) maximum error and CPU time (in seconds) of the test problem 3.

Size of the Matrices	Numerical Method	$E_{\max .}$	Time		
			Setup	Running	Total
16×16	FDM	6.9827e-04	2.3596e+00	8.1608e-02	2.4412e+00
	MGM	3.7003e-03	1.5288e-01	5.3050e-03	1.5819e-01
	HWMGM	2.3216e-04	5.0140e-02	4.3616e-03	5.4501e-02
	HWAMGM	2.1525e-06	4.6916e-02	4.9245e-03	5.1841e-02
64×64	FDM	2.1979e-04	2.2378e+00	8.0061e-02	2.3179e+00
	MGM	2.1205e-06	1.9227e-01	4.6270e-03	1.9690e-01
	HWMGM	7.8246e-05	7.3816e-02	4.8657e-03	7.8682e-02
	HWAMGM	2.8908e-08	7.2162e-02	4.0131e-03	7.6175e-02
256×256	FDM	5.2622e-06	8.3215e+00	1.6642e-01	8.4879e+00
	MGM	3.5508e-07	1.8339e-01	5.7750e-03	1.8916e-01
	HWMGM	1.3724e-06	9.5755e-02	8.2365e-03	1.0399e-01
	HWAMGM	5.4393e-10	8.7086e-02	1.3058e-02	1.0014e-01
1024×1024	FDM	3.7000e-07	4.2359e+00	1.2597e-01	4.3618e+00
	MGM	7.3719e-14	3.5539e-01	3.9648e-02	3.9504e-01
	HWMGM	6.4887e-08	2.8168e-01	4.4764e-02	3.2644e-01
	HWAMGM	7.1054e-14	2.3379e-01	4.5118e-02	2.7891e-01
4096×4096	FDM	1.0428e-07	5.8089e+02	2.3902e+00	5.8328e+02
	MGM	1.4211e-14	1.2238e+01	7.4630e-01	1.2984e+01
	HWMGM	2.2276e-10	1.0593e+01	7.1162e-01	1.1305e+01
	HWAMGM	1.2434e-14	1.0461e+01	7.0972e-01	1.1171e+01

of the lubrication problem is as follows, We know that the corresponding momentum equations are,

$$\frac{\partial}{\partial y}\left(\mu \frac{\partial w_1}{\partial y}\right) - \eta \frac{\partial^4 w_1}{\partial y^4} = \frac{\partial p}{\partial x}, \tag{4.7}$$

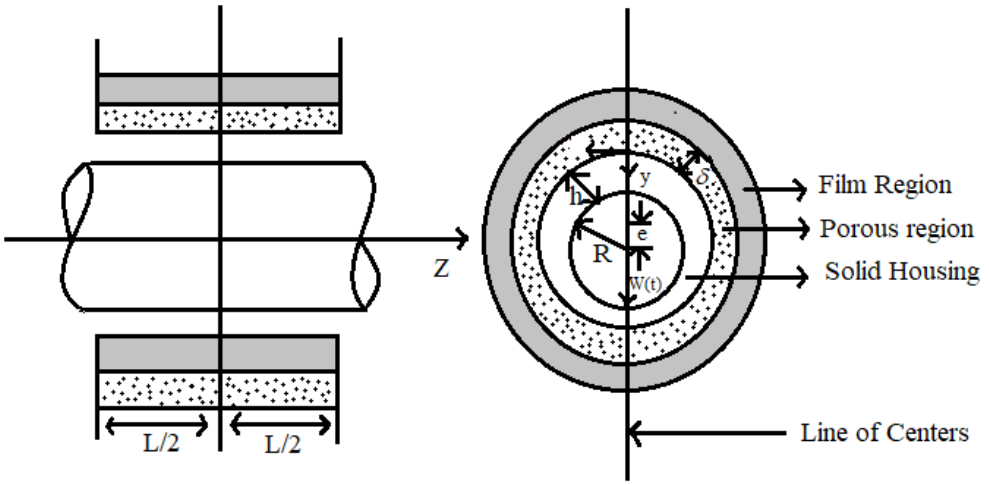

Figure 4. Physical configuration of the lubrication problem.

$$\frac{\partial}{\partial y}\left(\mu\frac{\partial w_3}{\partial y}\right) - \eta\frac{\partial^4 w_3}{\partial y^4} = \frac{\partial p}{\partial z}, \tag{4.8}$$

$$\frac{\partial p}{\partial y} = 0. \tag{4.9}$$

Here, μ represents the viscosity coefficient, w_1 is the velocity component of the lubricant along the x direction, η is the material constant responsible for couple stress property, and the velocities of the lubricant along y, z direction are represented by w_2 and w_3 respectively. Eq. (4.9) reveals the fact that there is no pressure along the y direction. The corresponding boundary conditions are (i) at $y = 0$,

$$w_1 = 0, w_2 = w_2^*, w_3 = 0, \tag{4.10}$$

$$\frac{\partial^2 w_1}{\partial y^2} = 0, \frac{\partial^2 w_3}{\partial y^2} = 0. \tag{4.11}$$

and (ii) at $y = h$,

$$w_1 = 0, w_2 = \frac{dh}{dt}, w_3 = 0, \tag{4.12}$$

$$\frac{\partial^2 w_1}{\partial y^2} = 0, \frac{\partial^2 w_3}{\partial y^2} = 0. \tag{4.13}$$

Here, h represents the film thickness, w_2^* representing the modified form of Darcy's velocity component along the y direction. When C being the minimum radial clearance and e is the eccentricity then, the equation of film thickness at any circumferential section θ becomes $h = C + e\cos(\theta)$. From the modified form of Darcy's law illustrate that the flow inside the porous region for couple stress fluid which accounts for polar effects is given by [38],

$$\vec{q}^* = \frac{-k}{\mu(1-B)}\nabla P^*, \tag{4.14}$$

where $\vec{q}^* = (w_1^*, w_2^*, w_3^*)$ is the modified Darcy velocity vector with $w_2^* = \frac{-k\delta}{\mu(1-B)}\frac{\partial P^*}{\partial y}$, and the modified Darcy velocity components along x, y, and z direction are respectively represented by w_1^*, w_2^*, and w_3^*. Also, the permeability of the porous material is represented by k, and the ratio

of microstructure size $\left(=\frac{\eta}{\mu}\right)$ to the pore size is expressed as $B=\frac{\frac{\eta}{\mu}}{k}$. The pressure in the porous region is represented by P^* and the couple stress parameter is represented by $l=\left(\frac{\eta}{\mu}\right)^{1/2}$.
The velocity components are obtained by solving Eqns. (4.7) and (4.8) by using the Eqns. (4.10)-(4.13) we have

$$w_1=\frac{1}{2\mu}\frac{\partial p}{\partial x}\left\{y\left(y-h\right)+2l^2\left(1-\frac{\cosh\left(\frac{2y-h}{2l}\right)}{\cosh\left(\frac{h}{2l}\right)}\right)\right\}, \tag{4.15}$$

$$w_3=\frac{1}{2\mu}\frac{\partial p}{\partial z}\left\{y\left(y-h\right)+2l^2\left(1-\frac{\cosh\left(\frac{2y-h}{2l}\right)}{\cosh\left(\frac{h}{2l}\right)}\right)\right\}. \tag{4.16}$$

We know that the equation of continuity as,

$$\frac{\partial w_1}{\partial x}+\frac{\partial w_2}{\partial y}+\frac{\partial w_3}{\partial z}=0. \tag{4.17}$$

Integrating Eq. (4.17) over film thickness 0 to h by substituting w_1, w_3 and after simplification we have

$$\frac{\partial}{\partial x}\left\{G\left(h,l\right)\frac{\partial p}{\partial x}\right\}+\frac{\partial}{\partial z}\left\{G\left(h,l\right)\frac{\partial p}{\partial z}\right\}=12\mu\frac{dh}{dt}+12\left.w_2^*\right|_{y=0}, \tag{4.18}$$

where $G\left(h,l\right)=h^3-12l^2\left(h-2l\tanh\left(\frac{h}{2l}\right)\right)$ and we have $\left.w_2^*\right|_{y=0}=\frac{-k}{\mu(1-B)}\left.\frac{\partial p^*}{\partial y}\right|_{y=0}$.
The pressure in the porous region P^* satisfies the Laplace equation,

$$\frac{\partial^2 P^*}{\partial y^2}=-\left(\frac{\partial^2 P^*}{\partial x^2}+\frac{\partial^2 P^*}{\partial z^2}\right) \tag{4.19}$$

Integrating Eq. (4.19) to analyze the pressure in a porous region, with respect to y over the porous layer of thickness H_0 and with the aid of the condition $\frac{\partial P^*}{\partial y}=0$ at $y=-H_0$. Also, by assuming that the surface at $y=0$ as the porous and at $y=-H_0$ as the non-porous and the pressure within the porous is taken as $p=P^*$. Then, we obtain the following equation,

$$\left.\frac{\partial P^*}{\partial y}\right|_{y=0}=-H_0\left(\frac{\partial^2 P^*}{\partial x^2}+\frac{\partial^2 P^*}{\partial z^2}\right). \tag{4.20}$$

Now from Eqns. (4.18) and (4.20), we obtain the squeeze film lubrication problem of porous journal bearings with coupe stress fluid in the following form,

$$\frac{\partial}{\partial x}\left\{\left(G\left(h,l\right)+\frac{12H_0k}{(1-B)}\right)\frac{\partial p}{\partial x}\right\}+\frac{\partial}{\partial z}\left\{\left(G\left(h,l\right)+\frac{12H_0k}{(1-B)}\right)\frac{\partial p}{\partial z}\right\}=12\mu\frac{dh}{dt}. \tag{4.21}$$

It is convenient to analyze by using the non-dimensional variables $\theta=\frac{x}{R}$, $\bar{z}=\frac{z}{l}$, $\varepsilon=\frac{e}{C}$, $\bar{h}=1+\varepsilon\cos\left(\theta\right)$, a $=\frac{L}{2R}$, $\bar{P}=\frac{pC^2}{\mu R^2\frac{d\varepsilon}{dt}}$, $\bar{l}=\frac{l}{C}$, $\frac{dh}{dt}=\frac{d\varepsilon}{dt}\cos\left(\theta\right))$, $S=\frac{kH_0}{C^3}$. From the above dimensionless terms, Eq. (4.21) can be reduced into the following form

$$\left(\bar{G}\left(\bar{h},\bar{l}\right)+\frac{12S}{(1-B)}\right)\frac{\partial^2\bar{P}}{\partial\theta^2}+F\left(\bar{h},\bar{l}\right)\frac{\partial\bar{P}}{\partial\theta}+\frac{1}{4a^2}\left\{\left(\bar{G}\left(\bar{h},\bar{l}\right)+\frac{12S}{(1-B)}\right)\frac{\partial^2\bar{P}}{\partial\bar{z}^2}\right\}+\frac{1}{4a^2}\left(M\left(\bar{h},\bar{l}\right)\frac{\partial\bar{P}}{\partial\bar{z}}\right)=12\cos\left(\theta\right). \tag{4.22}$$

Here, $\bar{G}\left(\bar{h},\bar{l}\right)=\bar{h}^3-12\bar{l}^2\left(\bar{h}-2\bar{l}\tanh\left(\frac{\bar{h}}{2\bar{l}}\right)\right)$, $F\left(\bar{h},\bar{l}\right)=\frac{\partial\left(\bar{G}\left(\bar{h},\bar{l}\right)\right)}{\partial\theta}$, and $M\left(\bar{h},\bar{l}\right)=\frac{\partial\left(\bar{G}\left(\bar{h},\bar{l}\right)\right)}{\partial\bar{z}}$
The pertinent boundary conditions are $\bar{P}=0$ at $\theta=\frac{\pi}{2},\frac{3\pi}{2}$, and $\bar{P}=0$ at $\bar{z}=\pm\frac{1}{2}$.
Applying the finite difference approximations to Eq. (4.22), we obtained the linear system and by using the HWAMGM presented in section 3, the obtained numerical solution of the lubrication

problem 4 is presented in Figure 5 with the varying ratio parameter $'a'$. Figure 6 represents the variation of non-dimensional pressure $\bar{P}$ obtained with the aid of HWAMGM with the varying couple stress parameter $\bar{l}$. The load carrying capacity is calculated and it is presented in Figure 7 and Figure 8 by varying the couple stress parameter $\bar{l}$ with the permeability parameter $S = 0.001$ and $S = 0.01$ respectively.

Pressure distribution of the Lubrication Problem:

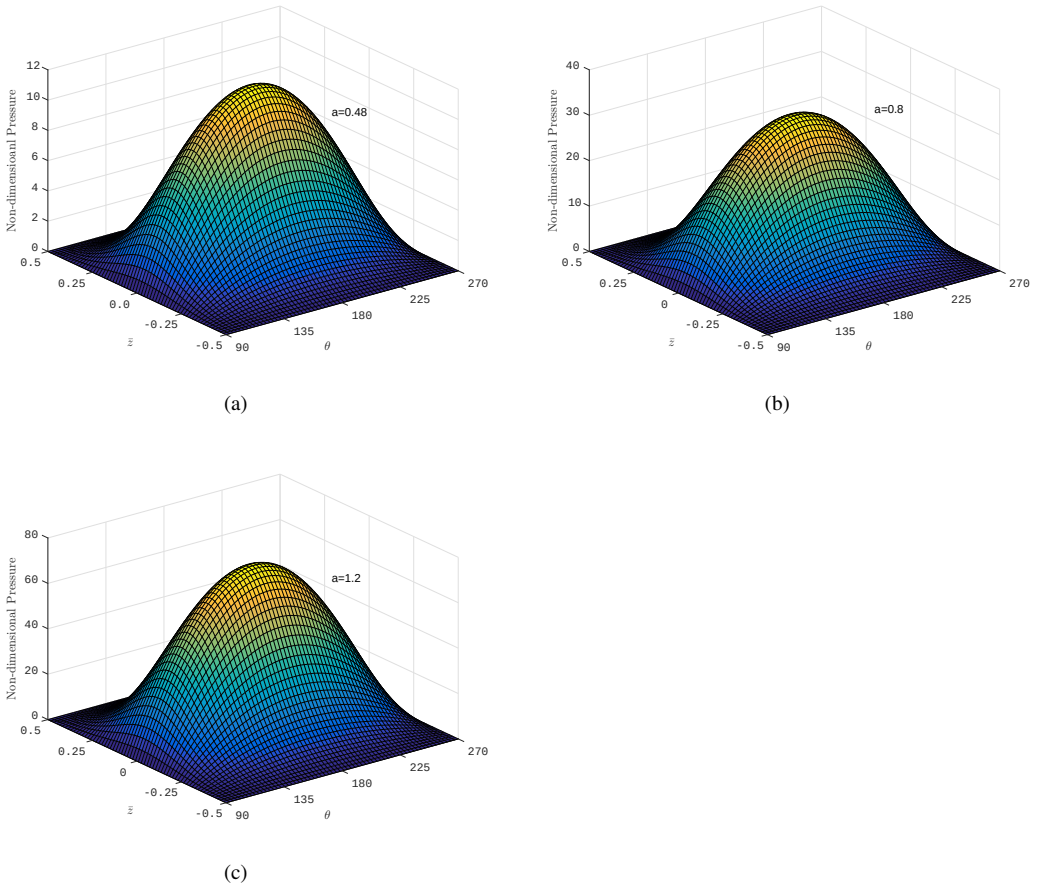

Figure 5. Non-dimensional pressure distribution for $\bar{l} = 0.2$, $B = 0.3$, $S = 0.001$, and $\varepsilon = 0.4$ at different values of a $((a)\ a = 0.48,\ (b)\ a = 0.8,\ (c)\ a = 1.2)$.

From Figure 5 we can observe that the non-dimensional squeeze film pressure distribution obtained by the HWAMGM is increased with the increasing values of the ratio parameter $'a'$.

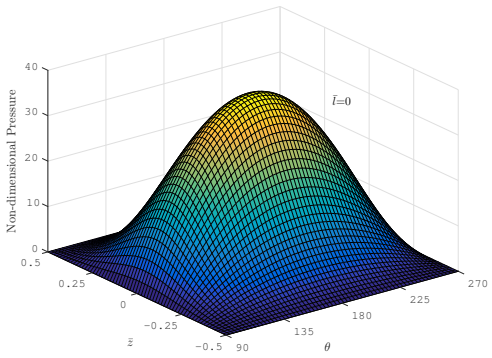

(a)

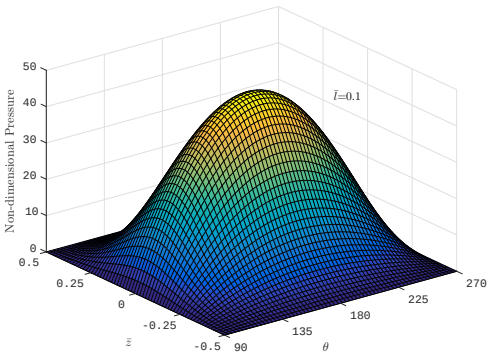

(b)

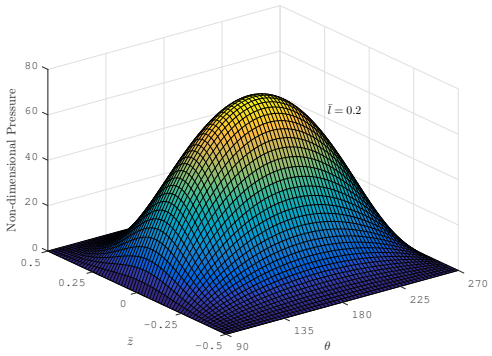

(c)

Figure 6. Non-dimensional pressure distribution for a $= 1.2$, $B = 0.3$, $S = 0.001$, and $\varepsilon = 0.4$ at different values of $\bar{l}$ ((i) $\bar{l} = 0$, (ii) $\bar{l} = 0.1$, (iii) $\bar{l} = 0.2$).

From Figure 6 we can observe that the non-dimensional squeeze film pressure distribution obtained by the HWAMGM is increased with the increasing values of the couple stress parameters $\bar{l}$.

Load-carrying capacity: The variation of the load-carrying capacity of the lubrication problem 4 is given by,

$$Load = \Delta\theta.\Delta\bar{z}\sum_{i=1}^{J}\sum_{j=1}^{J}\bar{P}_{i,j}\cos(\theta_i)$$

The non-dimensional pressure obtained by the HWAMGM is used to calculate the load-carrying capacity variation with respect to eccentricity ratio ε, as shown in Figure 7. In addition, we can see in Figure 7 that as the couple stress parameter is increased, the load capacity increases.

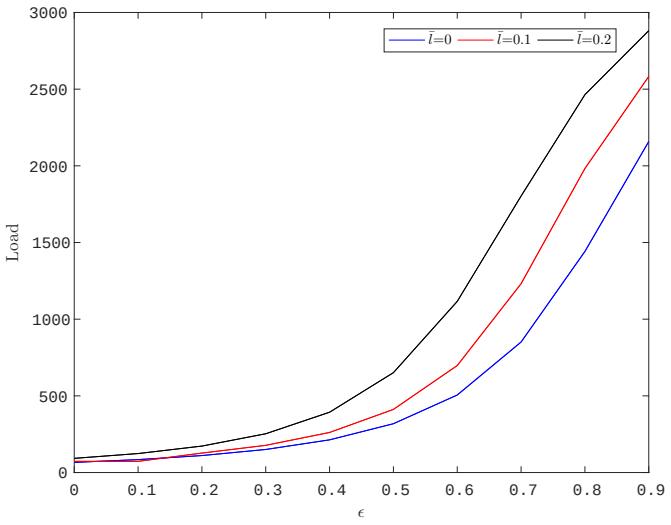

Figure 7. The variation of load capacity for a $= 0.48,\ B = 0.3,$ and $S = 0.001$ at different values of $\bar{l}$.

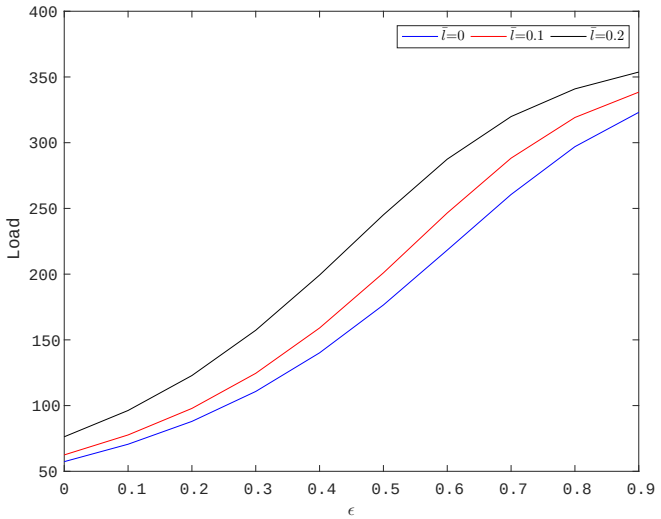

Figure 8. The variation of load capacity for a $= 0.48,\ B = 0.3,$ and $S = 0.01$ at different values of $\bar{l}$.

Figure 8 represents the variation of load capacity with respect to eccentricity ratio ε. Also, from Figure 8 it is observed that the load capacity increases with increasing values of couple stress parameter.

5 Conclusion

In this article, we have provided an effective Haar wavelet algebraic multigrid method (HWAM GM) to solve the modified Reynolds equation corresponding to the squeeze film lubrication of finite porous journal bearing with the couple stress fluid as a lubricant. This method initially reduces the modified Reynolds equation to a system of linear algebraic equations. To minimize the error associated with this linear system, the Haar wavelet filters based multigrid operators are used. Moreover, the results obtained are compared with the FDM, MGM, and HWMGM for three numerical examples having the exact solutions. From the obtained solutions we ob-

served that the HWAMGM solutions are well compared with the exact solution for increasing the value of J (resolution of the Haar wavelet) with lesser computational CPU time. Due to the high accuracy with a lesser computational time of the proposed method can be extended to analyze the pressure distribution and the load-carrying capacity in porous journal bearing by solving the corresponding non-dimensional modified Reynolds equation, and it is observed that the squeeze film pressure distribution increases with increasing the values of ratio parameter and couple stress parameter. Also, as the values of the couple stress parameter are increased, the load capacity increases. Finally, it is predicted that the projected method can be set up comprehensively and suitable for the solution of various types of equations that arise in Hydrodynamic lubrication theory.

References

[1] V. Wright and D. Dowson, Lubrication and cartilage, *J. Anat.* **121**, 107–118 (1976).

[2] O. Pinkus and B. Sternlicht, *Theory of hydrodynamic lubrication*, McGraw- Hill, New York, (1961).

[3] A. Cameron, *The principles of lubrication*, Longmans, London, (1966).

[4] B. J. Hamrock, *Fundamentals of fluid film lubrication*, McGraw-Hill, New York, (1994).

[5] J. S. Hou, V. C. Mow, W. M. Lai and M. H. Holmes, An analysis of the squeeze-film lubrication mechanism for articular cartilage, *J. Biomechanics* **25**, 247–259 (1992).

[6] C. Cusano, Lubrication of porous journal bearings, *J. Lubr. Technol.* **94(1)**, 69–73 (1972).

[7] J. Prakash and S. K. Vij, Load capacity and time-height relations for squeeze films between porous plates, *Wear* **24(3)**, 309–315 (1973).

[8] H. Wu, An analysis of squeeze film between porous rectangular plates, *J. Lubr. Technol.* **94(1)**, 64–68 (1972).

[9] V. T. Morgan and A. Cameron, Mechanism of Lubrication in Porous Metal Bearings, *Conf. Lubr. Wear London*, 151–157 (1957).

[10] C. A. Rhodes and W. T. Rouleau, Hydrodynamic lubrication of narrow porous metal bearings with sealed ends, *Wear* **8**, 474–486 (1965).

[11] C. A. Rhodes and W. T. Rouleau, Hydrodynamic lubrication of partial porous metal bearings, *J. Basic Eng.* **88(1)**, 53–60 (1966).

[12] E. Capone, Lubrication of axially undefined porous bearings, *Wear* **15(3)**, 157–170 (1970).

[13] K. C. Patel and J. L. Gupta, Hydrodynamic lubrication of a porous slider Bearing with slip velocity, *Wear* **85**, 309–317 (1983).

[14] M. V. Bhat, Hydrodynamic Lubrication of a Porous Composite Slider Bearing, *Jpn. J. Appl. Phys.* **17(3)**, 479–481 (1978).

[15] G. D. Smith, *Numerical solution of partial differential equations: Finite difference methods*, Oxford Univ. Press, New York, (1985).

[16] C. Johnson, *Numerical solutions of partial differential equations by the finite element method*, Cambridge Univ. Press, Cambridge, New York, (1987).

[17] W. L. Briggs, V. Henson and S. F. McCormick, *A Multigrid Tutorial*, J. Soc. Ind. Appl. Math., Philadelphia, (2000).

[18] Z. Huang and Q. Chang, Gauss-Seidel type multigrid methods, *J. Comput. Math.* **21(4)**, 421–434 (2003).

[19] K. Stüben, Algebraic Multigrid (AMG): Experiences and Comparisons, *Appl. Math. Comput.* **13(3-4)**, 419–451 (1983).

[20] A. Brandt, Algebraic Multigrid Theory: The Symmetric Case, *Appl. Math. Comput.* **19**, 23–56 (1986).

[21] F. H. Pereira, S. L. Verardi and S. I. Nabeta, A fast algebraic multigrid preconditioned conjugate gradient solver, *Appl. Math. Comput.* **179**, 344–351 (2006).

[22] Ü. Lepik, Numerical solution of evolution equations by the Haar wavelet method, *Appl. Math. Comput.* **185**, 695–704 (2007).

[23] S. C. Shiralashetti and P. Badiger, Chebyshev wavelets approach for the squeeze film lubrication of long porous journal bearings with couple stress fluids, *Malaya j. mat.* **S(1)**, 138–143 (2020).

[24] Ö. Oruç, A computational method based on Hermite wavelets for two-dimensional Sobolev and regularized long wave equations in fluids, *Numer. Methods Partial Differ. Equ.* **00**, 1–23 (2017).

[25] W. L. Briggs and V. E. Henson, Wavelets and Multigrid, *J. Sci. Comput.* **14(2)**, 506–510 (1993).

[26] A. Avudainayagam and C. Vani, Wavelet based multigrid methods for linear and nonlinear elliptic partial differential equations, *Appl. Math. Comput.* **148**, 307–320 (2004).

[27] D. D. Leon, A new wavelet multigrid method, *J. Comput. Appl. Math.* **220**, 674–685 (2008).

[28] S. C. Shiralashetti, M. H. Kantli and A. B. Deshi, A new wavelet multigrid method for the numerical solution of elliptic type differential equations, *Alex. Eng. J.* **57**, 203–209 (2018).

[29] S. C. Shiralashetti, L. M. Angadi and A. B. Deshi, Biorthogonal wavelet-based multigrid and full approximation scheme for the numerical solution of parabolic partial differential equations, *Asian-Eur. J. Math.* **12(1)**, 1–20 (2019).

[30] S. C. Shiralashetti and L. M. Angadi, Numerical solution of some class of nonlinear partial differential equations using wavelet-based full approximation scheme, *Int. J. Comput. Methods* **17(6)**, 1950015 (2020).

[31] V. M. Garcia, L. Acevedo and A. M. Vidal, Variants of algebraic wavelet-based multigrid methods: Application to shifted linear systems, *Appl. Math. Comput.* **202**, 287–299 (2008).

[32] P. J. Vanfleet, *Discrete wavelet transformation an elementary approach with applications*, Wiley Inter science, Hoboken, New Jersey, (2008).

[33] F. H. Pereira, S. L. Verardi and S. I. Nabeta, A wavelet-based algebraic multigrid preconditioner for sparse linear systems, *Appl. Math. Comput.* **182**, 1098–1107 (2006).

[34] Y. Saad and M. H. Schultz, GMRES: A generalized minimal residual algorithm for solving non symmetric linear systems, *SIAM J. Sci. Stat. Comput.* **7(6)**, 856–869 (1986).

[35] I. E. Lagaris, A. Likas and D. I. Fotiadis, Artificial Neural Networks for solving ordinary and partial differential equations, *IEEE Trans. Neural Netw.* **9(5)**, 987–1000 (1998).

[36] Y. Yang, M. Hou, H. Sun, T. Zhang, F. Weng and J. Luo, Neural network algorithm based on Legendre improved extreme learning machine for solving elliptic partial differential equations, *Soft Comput.* **24**, 1083–1096 (2020).

[37] V. K. Stokes, Couple-stresses in fluids, *Phys. Fluids* **9**, 1709–1715 (1966).

[38] N. B. Naduvinamani and A. Siddanagouda, Combined effects of surface roughness and couple stresses on squeeze film lubrication between porous circular stepped plates, *Proc. Instn. Mech. Int. Mech. J. Eng. Tribol.* **221**, 525–534 (2007).

Author information

S. C. Shiralashetti and Praveenkumar Badiger, P. G. Department of Studies in Mathematics, Karnatak University, Dharwad-580003, Karnataka, India.
E-mail: scshiralashetti@kud.ac.in

Received: 2021-11-20.
Accepted: 2022-04-04.